

Guided transport of ultracold gases of rubidium up to a room-temperature dielectric surface

A L Marchant, S Händel, T P Wiles, S A Hopkins and S L Cornish

Department of Physics, University of Durham, South Road, Durham DH1 3LE, UK

E-mail: a.l.marchant@durham.ac.uk

Abstract.

We report on the guided transport of an atomic sample along an optical waveguide up to a room-temperature dielectric surface. The technique exploits a simple hybrid trap consisting of a single beam dipole trap positioned $\sim 125\ \mu\text{m}$ below the field zero of a magnetic quadrupole potential. Transportation is realised by applying a moderate bias field ($<12\ \text{G}$) to displace the magnetic field zero along the axis of the dipole trap. We use the technique to demonstrate that atomic gases may be precisely positioned at controlled distances from the surface with negligible heating or loss. This work forms an excellent basis for future studies of atom-surface interactions using ultracold atomic gases.

PACS numbers: 04.80.Cc, 05.60.Cd, 06.60.Sx, 07.05.Fb, 37.10.Gh, 37.25.+k

1. Introduction

Understanding the fundamental forces which govern the world around us has long been a challenge for the scientific community. Of particular interest is the search for a comprehensive explanation of gravity. Newton published his theory of gravitation in 1687 [1] and since then attempts to experimentally verify its proposal have covered length scales from the astronomical [2] to the sub millimetre [3]. The results of such experiments have not only fundamental significance, but also important technological implications.

Although these experiments seek to, and have imposed, increasingly strict bounds on fundamental forces there are still many open questions regarding the possibility of short-range corrections to gravity which extend beyond the Standard Model. Despite the electromagnetic, strong and weak forces all being well described by quantum field theories, the current description of gravity set out by Einstein's theory of general relativity, which reduces to Newtonian gravity on everyday length scales, breaks down in the quantum limit and as such, is currently excluded from the Standard Model. As a starting point, many experiments look for deviations from the expected inverse square law, with new forces instead being characterised by a Yukawa type potential of the form

$$U(r) = \frac{-G_N m_1 m_2}{r} (1 + \alpha e^{-r/\lambda}), \quad (1)$$

where α is the strength of the force and λ its range. At the 1 μm level current experimental constraints permit these forces to be as large as 10^{10} times Newtonian gravity [4].

Attempts to measure the gravitational attraction between two masses have improved dramatically from the first experiments by Cavendish in 1798 [5] and now vary widely in approach from superconducting gravity gradiometers [6] and microcantilevers [7] to planar oscillators [8] and torsion balance experiments [9]. However in scaling down experiments to probe ever decreasing length scales a new, fundamental problem arises. Quantum electrodynamics predicts a macroscopic force between conductors, known as the Casimir force [10]. This force vastly overwhelms the much weaker gravitational attraction between the test masses, such that experiments are forced to search for deviations between the theoretical and experimental Casimir forces. However, precisely calculating such Casimir forces for a specific macroscopic test mass near a surface is generally difficult [11]. In contrast the interaction between a single neutral atom and a plane surface is well understood [12, 13] being characterised by the attractive Casimir-Polder potential,

$$U_{\text{CP}} = \begin{cases} U_{\text{vdW}} = -\frac{C_3}{x^3} & \text{for } x < \lambda_{\text{opt}}/2\pi \\ U_{\text{ret}} = -\frac{C_4}{x^4} & \text{for } \lambda_{\text{opt}}/2\pi < x < \lambda_{\text{T}} \end{cases} \quad (2)$$

$$(3)$$

where for longer length scales the $1/x^3$ form of the van der Waals potential, characterised by C_3 , becomes $1/x^4$ due to retardation effects. This new regime is characterised by

C_4 with the transition point between the two regimes determined by the wavelength corresponding to the excitation energies of the interacting atoms, λ_{opt} [14]. Further from the surface (larger than the thermal wavelength of photons, λ_T) the interaction becomes dominated by the thermal fluctuation of the electromagnetic field [15]. In our case these length scales are $\lambda_{\text{opt}}/2\pi \approx 0.12 \mu\text{m}$ and $\lambda_T \approx 7.6 \mu\text{m}$.

The inherent advantage of directly probing the atom-surface interaction has prompted the recent proposal of a new generation of experiments which aim to exploit the precision and control offered by atomic physics and ultracold quantum gases to push the measurement of short-range forces into a new regime [16–19]. Indeed a number of proof-of-principle experiments have already utilised ultracold atomic gases to explore the short range van der Waals and Casimir-Polder potentials [20–23]. Nevertheless such experiments are in their infancy and considerable refinement is required before they become competitive with the classical ‘Cavendish style’ experiments as a test of short-range gravitational forces.

Common to all these new atomic physics experiments is the need to controllably manipulate ultracold atoms near a room-temperature surface. Here we report the development of a new apparatus designed to study such atomic samples in close proximity to a room-temperature dielectric surface. In particular we describe and analyse a simple technique for the guided transport of an ultracold atomic gas along an optical waveguide. Our approach uses a hybrid optical and magnetic trap formed from a single optical dipole trap positioned $125 \mu\text{m}$ below the field zero of a magnetic quadrupole potential (see figure 1(a)-(c)). This simple hybrid trap allows us to position the sample precisely along the optical waveguide by the application of a moderate bias field to displace the field zero of the quadrupole potential. In this paper, we demonstrate the ability to bring ultracold atomic samples of ^{87}Rb up to the surface and investigate the effect of the surface potential on the trapped sample.

For future work our experimental geometry is such that atoms can be controllably launched horizontally towards the test surface using the dipole beam as a waveguide hence it is possible to obtain a low incident velocity perpendicular to the surface without requiring the atoms approach at grazing incidence as in some previous experiments [24, 25]. The use of a fused silica dove prism as the experimental surface permits the creation of an evanescent wave barrier at the prism face hence the system has clear applications for studies of both classical and quantum reflection from a solid surface.

2. Modelling the trap potential

It is important to fully understand the hybrid potential formed by the combined magnetic and optical trap if atoms are to be translated up to and away from the surface in a controlled way. The total potential seen by the atoms has four contributions,

$$U_{\text{total}} = U_{\text{dipole}} + U_{\text{mag}} + U_{\text{g}} + U_{\text{CP}}, \quad (4)$$

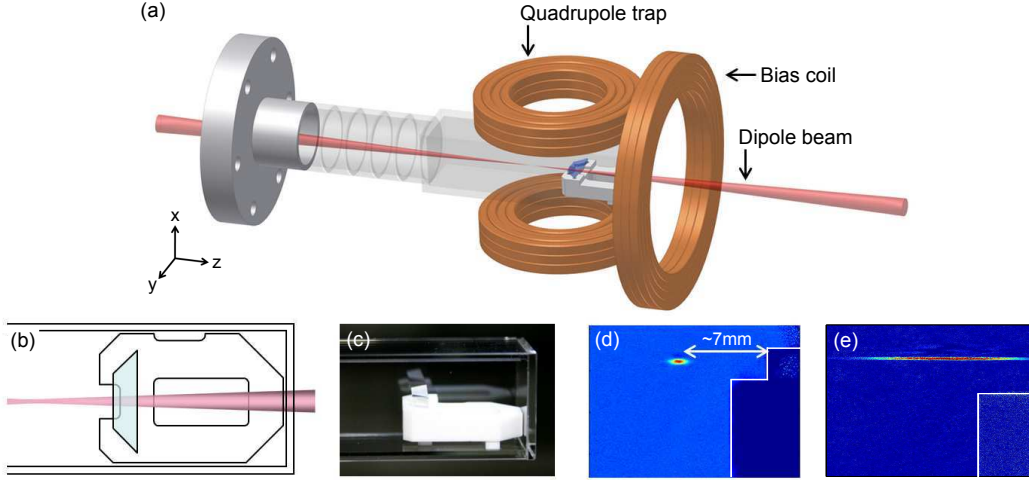


Figure 1. Experimental setup: (a) Trapping geometry near the surface. A single dipole beam is delivered through the back surface of the glass prism, focussing 3.5 mm from its front surface. Axial confinement along the beam is provided by a magnetic quadrupole field. A single coil positioned behind the prism is used to produce a bias field to shift the location of the quadrupole field zero along the beam direction. (b) Schematic of the glass cell, the dove prism, the macor prism mount and the dipole beam from above. (c) Photograph of the prism within the glass cell. (d) False colour absorption image of atoms trapped near the prism surface. (e) False colour absorption image of atoms in the waveguide without magnetic confinement.

where U_{dipole} is the optical dipole potential, U_{mag} is the magnetic potential (consisting of both the quadrupole and bias fields), U_g is the earth's gravitational potential and U_{CP} is the potential produced by the atom-surface interaction. This net potential is depicted in figure 2 (a) for a trap positioned far from the surface.

The optical contribution to the trap potential is modelled as a sum over any significant transitions from the ground state according to,

$$U_{\text{dipole}} = 3c^2 \left(\sum_i \frac{\Gamma_i}{\Delta_i \omega_{0i}^3} \right) \frac{P}{w^2(z)} \exp \left(-\frac{2r^2}{w^2(z)} \right). \quad (5)$$

Here Γ_i is the natural linewidth, Δ_i is the laser detuning, ω_{0i} is the transition frequency, P is the power of the dipole beam propagating in the z direction, $w(z)$ is the beam size, given by $w(z) = w_{0M} [1 + (z\lambda M^2 / \pi w_{0M}^2)^2]^{1/2}$ (where w_{0M} is the $1/e^2$ radius at the beam waist), and r is the radial distance from the beam centre. In our case the dipole beam is derived from a $\lambda=1030$ nm Yb disk laser and is focussed to a waist of $57 \mu\text{m}$ with an $M^2 = 1.06$ and Rayleigh range $z_R = 9.9$ mm. This beam is positioned $125 \mu\text{m}$ below the field zero created by a magnetic quadrupole trap. The quadrupole gradient is usually set to approximately cancel gravity (30.6 Gcm^{-1} for ^{87}Rb in the $F = 1, m_F = -1$ state) hence the full trap depth is determined by the dipole beam alone. This is due to an effective cancellation of the gravitational and magnetic potentials in equation (4) below the field zero. In contrast, above the field zero, the trapping potential and the gravitational acceleration terms add to produce a tilted trap which lowers the potential

barrier and hence trap depth as shown in figure 2 (b).

2.1. Case I: Idealised transport in the hybrid trap

In this hybrid trap configuration tight radial confinement is created by the dipole beam. Axial confinement along the beam is provided by the quadrupole field. (Without any magnetic confinement the cloud extends along the waveguide, centred around the beam waist, due to the low (~ 2 Hz) axial trap frequency produced by the dipole beam alone as shown in figure 1 (e).) The axial potential produced by the quadrupole field is harmonic for $z \ll x_{\text{offset}}$ (where x_{offset} is the vertical separation between the beam and field zero) and linear otherwise. The harmonic trap frequency is determined by the quadrupole gradient and the vertical displacement of the beam from the field zero [26]. Figure 2 (c) shows how the axial trap frequency evolves as the dipole beam is moved further, vertically, from the field zero when the quadrupole gradient is such that atoms are supported against gravity. In this hybrid trap the position of the atoms along the dipole beam is determined not by the beam waist but instead by the location of the quadrupole trap centre. The application of a horizontal bias field parallel to the dipole beam produces a shift of the field zero along the same line. In this way atoms can be transported along the length of the dipole beam and up to the prism surface.

2.2. Case II: Transport with an offset bias field

In the idealised case the application of the bias field moves the field zero purely along the z axis thus keeping the distance between the dipole beam and the field zero, and hence the axial trap frequency, constant. However, due to physical constraints of the apparatus it is unfeasible to position a pair of bias coils symmetrically about the beam. Instead we must use a single coil, displaced 17 cm in the z direction from the field zero. Additionally the symmetry axis of the coil is offset 1.5 cm vertically. Theoretically accounting for the offset of the bias coil produces small deviations from the trapping expected for displacement along a gaussian beam. This is the result of the trajectory taken by the field zero as the bias field is increased due to a non-axial magnetic field component produced by the offset of the bias coil. As shown in figure 2 (c) any vertical displacement translates into a change in axial trap frequency. The theoretical model of this axial frequency change is shown, along with experimentally determined values, in section 3.3.

3. Production of ultracold gases near a dielectric surface

3.1. Loading the hybrid trap

To prepare the atomic sample ^{87}Rb atoms are loaded from a magneto-optical trap (MOT) into a quadrupole trap mounted on a motorised translation stage. Once loaded, this quadrupole trap is moved horizontally, transporting the atoms towards a second,

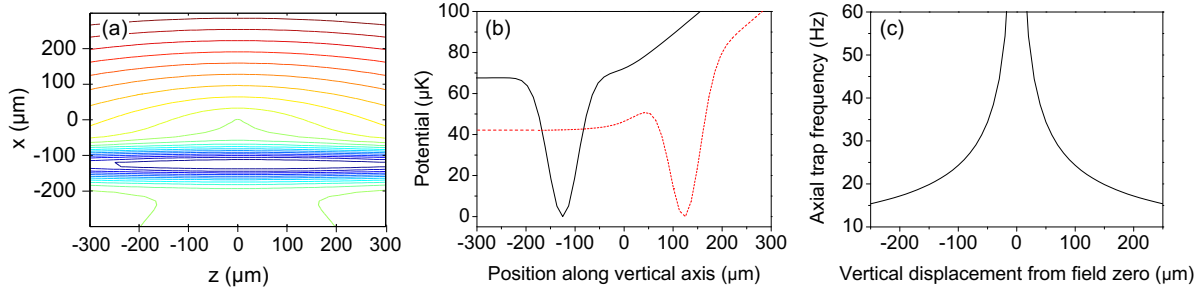


Figure 2. The hybrid trap: (a) Equipotential of the hybrid trap in the plane $y = 0$. (b) The potential obtained in the x direction for a magnetically levitated trap with the dipole beam positioned $125 \mu\text{m}$ below (solid, black line) and $125 \mu\text{m}$ above (red, dashed line) the magnetic field zero. (c) Axial trap frequency as a function of vertical beam displacement from the magnetic field zero.

static quadrupole trap (shown in figure 1 (a)) into which the atoms are transferred. The atoms are then further cooled by forced RF evaporation resulting in a sample of 2.7×10^7 atoms at a temperature of $32 \mu\text{K}$. Further details of the apparatus are presented in [27, 28].

To load the hybrid dipole trap the quadrupole gradient is relaxed from 192 G cm^{-1} down to 29.3 G cm^{-1} in 1 s. The combined potential produced by the dipole beam and quadrupole field results in trap frequencies of $\omega_r = 2\pi \times 480 \text{ Hz}$ and $\omega_z = 2\pi \times 24 \text{ Hz}$ at the beam waist. After loading, the cloud rapidly equilibrates to around $U_0/10$, where U_0 is the depth of the trap (this fraction we experimentally verify in section 3.3), roughly $7 \mu\text{K}$. Further evaporation can then be performed by reducing the beam intensity. Throughout all experiments the dipole trap waist is positioned 3.5 mm from the super-polished room-temperature dielectric prism. Initially the quadrupole trap centre is located 6.8 mm from the prism surface, as shown in figure 1(d). This geometry was chosen such that in moving up to the surface the cloud is always confined less than half a Rayleigh range from the beam waist, leading to minimal variation in the radial trapping potential. The cloud can be moved closer to and further from the prism by application of the bias field (where a positive displacement moves the cloud from the initial quadrupole trap centre, closer to the surface) as shown in figure 3. The magnitude of this shift is given by,

$$z = \frac{B_0}{B'_z/2} \quad (6)$$

where B_0 is the applied bias field and B'_z is the axial quadrupole field gradient. For the (approximately) levitated potential the use of $-12 \text{ G} \leq B_0 \leq 12 \text{ G}$ produces displacements of $-8.2 \text{ mm} \leq z \leq 8.2 \text{ mm}$, on the order of a Rayleigh range ($z_R = 9.9 \text{ mm}$).

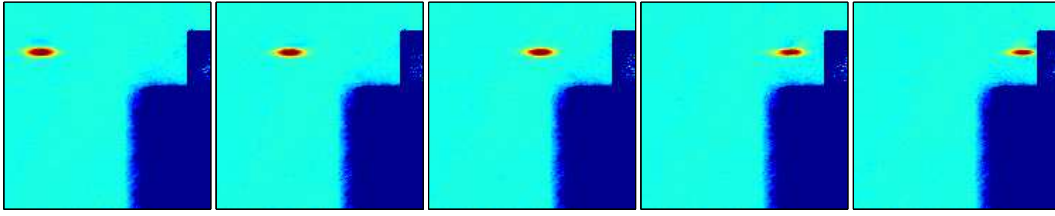


Figure 3. False colour absorption images of atoms approaching the surface. Bias fields applied range from 0 G to 10 G. To the right on each image the glass prism can be seen sharply defined on top of its macor mount (unfocussed edges).

3.2. Speed of transport

The maximum speed of the cloud transport without setting up sloshing in the trap is governed by the magnetic field gradient used to close the ends of the dipole beam. Ideally the bias field ramp should be adiabatic to reduce any heating effects. This was experimentally verified by measuring the amplitude of the oscillation induced by the transportation. In order to map out the oscillation absorption images of the cloud were taken after quarter trap period time steps for atoms at temperatures of $1.5 \mu\text{K}$ and $7 \mu\text{K}$. Figure 4 (a) shows that to complete a shift of 4.2 mm without setting up an oscillation requires a ramp time of ~ 2.5 s. As expected, this is independent of cloud temperature. In principle this time can be reduced with the use of a tighter field gradient at the expense of requiring a higher bias field.

3.3. Characterisation of the hybrid trapping potential: A ‘single-shot’ diagnostic

With the flexibility to displace the trap centre anywhere along the beam, it is possible to use the trapped atoms to characterise the profile of the dipole beam. We use a ‘single-shot’ diagnostic routine to measure important trap properties quickly and reliably. This approach is suitable when high trap frequencies are used, for example in single beam dipole traps. After a time of flight, τ_{TOF} , the width of the cloud, σ_i , is given by

$$\sigma_i^2 = \left(\frac{kT}{m\omega_i^2} \right) (1 + \omega_i^2 \tau_{\text{TOF}}^2). \quad (7)$$

In the limit that $\omega_i \tau_{\text{TOF}} \gg 1$, i.e. in the case of the radial trap frequency, the cloud width after time of flight is governed only by the cloud temperature and not the frequency of the trap at release. Hence it is possible to determine the cloud temperature without prior knowledge of the trapping potential in a single shot. The axial trap frequency can then simply be calculated from the axial cloud size and the temperature as determined from the radial size. If the cloud is held in the trap sufficiently before release such that the gas reaches full thermal equilibrium with the potential the radial trap frequency can also be derived from this measurement; knowledge of the dipole trap beam power together with the assumption that the cloud equilibrates to some fraction the trap depth, $1/\eta$, (which we establish later in this section) allows the $1/e^2$ beam radius and hence the radial trap frequency to be determined from the temperature measurement.

Such measurements are found to be in good agreement with the values obtained from parametric heating. This method allows the position of the beam waist to be located precisely and the distance between the magnetic field zero and the dipole beam to be determined over the full range of transport distances.

Figure 4 (b) shows the effect of transport along the beam on atom number for a cloud initially allowed to come into thermal equilibrium with the trapping potential through evaporation. For shifts sufficiently far from the prism such that the atoms do not interact with the surface, there is no detectable atom loss. Closer to the prism the attractive Casimir-Polder potential opens up the trap, see inset figure 5 (a), leading to a sharp drop in the atom number, the red (open) circles. The effect of the same transport on the cloud temperature is shown figure 4 (c). The observed temperature change is due simply to the adiabatic compression and relaxation of the cloud as the radial trapping potential varies along the optical waveguide and not as a result of a heating mechanism associated with the motion of the cloud. Knowing the beam power at the trap and the beam waist (determined from parametric heating measurements) it is possible to model the trap depth along the waveguide. The solid line in figure 4 (c) demonstrates that the temperature data are consistent with a cloud in thermal equilibrium with the trapping potential for $\eta \approx 9$. Note again the two red (open) circles correspond to a shift sufficient for the surface potential to open up the trap, hence reducing the trap depth and leading to atom loss. As such, we do not expect agreement with the model potential for these points. To test explicitly for heating due to the transport, measurements were performed shifting a cloud cooled to $1/20$ of the trap depth to suppress evaporation. Under such conditions some moderate heating was observed dependent on the speed and distance of the transport. However, the fact that the cloud remains in thermal equilibrium with the trapping potential (figure 4 (c)) and the absence of any atom loss (figure 4 (b)) demonstrates that this does not prohibit efficient transport of the atoms.

Analysis of the measured axial trap frequency moving along the beam confirms the theoretical prediction (solid line figure 4 (d)) that the vertical distance between the beam and the magnetic field zero does not remain constant when applying a bias field as a result of the bias coil's spatial offset from the beam axis. This leads to the small but measurable variation in trap frequency evident in figure 4 (d). However, this would be eliminated with a coil arrangement producing a field in the axial direction only.

4. Loss due to the surface

It is remarkable that trapped atoms at a temperature of a few μK can be brought close to a surface at 300 K. Atoms that collide with the surface can be adsorbed or reemitted at room temperature speeds, however the cloud density is low enough that this does not cause further losses from the trapped sample. Indeed the hot surface may be used as a knife for evaporative cooling [29]. Here we demonstrate how the atom loss caused by a controlled contact with the surface can be used to infer properties of the cloud such as size and temperature.

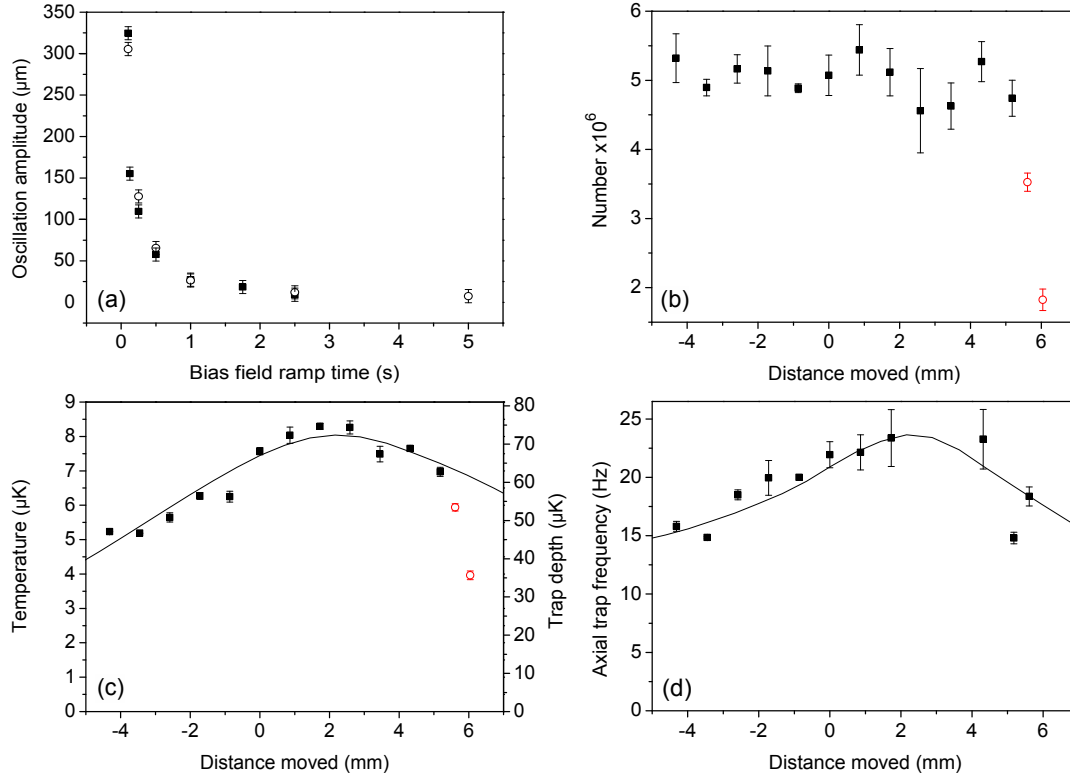


Figure 4. Characterisation of the transportation: (a) Oscillation set up by shifting the cloud 4.2 mm by displacement of the magnetic field zero in different lengths of time. Filled squares are for a cloud at 1.5 μK . Open circles are for a cloud at 7 μK . (b) Atom number as a function of horizontal trap shift caused by movement of the quadrupole field zero along the dipole beam. Red circles are for clouds sufficiently close to the surface that atoms are lost due to the atom-surface interaction opening up the trapping potential. (c) Vertical cloud temperature as a function of horizontal trap shift. Red circles are for clouds sufficiently close to the surface that atom loss from the cloud becomes a factor in the temperature. Solid line: Theoretical trap depth calculated from known dipole and quadrupole trap properties, accounting for an off axis bias field. Note the scale is $\times 9$ that of the experimental data indicating $\eta = 9$ (see text). (d) Experimentally determined axial trap frequency derived from the radial temperature and axial size of the cloud after time of flight. Solid line: Theoretical axial trap frequency calculated from known dipole and quadrupole trap properties, accounting for off axis bias field. Displacements are with reference to the initial quadrupole trap centre location with no applied bias field.

Atoms are loaded into the hybrid trap with no initial bias field and allowed to equilibrate to 7 μK . The bias field is then ramped to the necessary level in 5 s. Following this, the cloud is held at the shifted location for 50 ms (on the order of one axial trap period) before being shifted away from the surface a short distance and imaged. The displacements shown in figure 5 (a) are from the initial quadrupole trap location at zero bias field. In the case of the colder cloud (1.4 μK) an evaporation ramp in the dipole trap is first applied before the cloud is displaced along the beam. To produce the coldest cloud near the surface (0.3 μK) an initial dipole evaporation stage is carried out and the

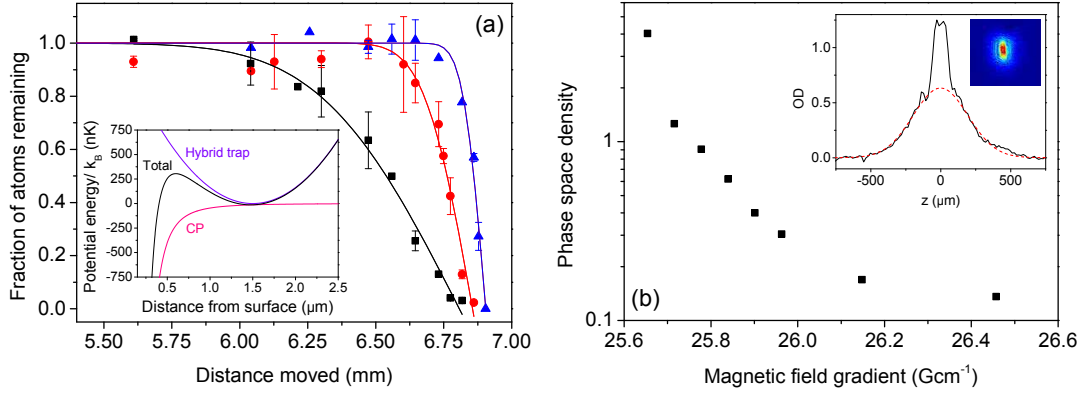


Figure 5. Atoms near the surface: (a) Atom loss as a function of displacement from the initial quadrupole trap position for cloud temperatures of $7.0 \mu\text{K}$ (black squares), $1.4 \mu\text{K}$ (red circles) and $0.3 \mu\text{K}$ (blue triangles). Fitted lines are of the form $N = N_0 \text{erf}((z - z_0)/(\sqrt{2}\sigma))$ for $z > z_0$. Inset: Total trapping potential resulting from the hybrid trap and atom-surface potentials near the prism. (b) Phase space density as a function of magnetic field gradient for a fixed dipole beam intensity for a cloud initially positioned to be just in contact with the surface. Inset: Cross section through a cloud, initially at $1.5 \mu\text{K}$ and a phase space density of 2×10^{-2} , following evaporation to degeneracy using the surface. The false colour image shown is after 40 ms levitated time of flight.

cloud is shifted (6 mm) close to the prism before a further evaporation stage is employed to reach the final temperature.

Far away from the surface the atomic cloud is unperturbed by displacement along the beam. Once the atomic cloud is sufficiently close to be able to interact with the surface, atom loss is observed along with a decrease in temperature. This interaction occurs at smaller trap centre - prism separations for colder clouds.

For harmonic axial confinement, it is possible to fit the atom loss as function of displacement using an error function of the form

$$N = N_0 \text{erf} \left(\frac{z - z_0}{\sqrt{2}\sigma} \right), \quad (8)$$

for $z > z_0$ where N is the number of atoms remaining at a given distance, N_0 is the initial atom number far from the surface, z is the distance shifted to, z_0 is the location of the cutting surface and σ is the cloud width given by $\sigma = (kT/m\omega_z^2)^{1/2}$. From this fit we find the cloud widths to be $400(20) \mu\text{m}$ ($7.0 \mu\text{K}$ cloud), $140(20) \mu\text{m}$ ($1.4 \mu\text{K}$ cloud) and $65(6) \mu\text{m}$ ($0.3 \mu\text{K}$ cloud) where the given temperatures are determined from time of flight expansion. Converting these widths to temperatures we find reasonable agreement with the time of flight data for the colder clouds. For the larger clouds the anharmonic nature of the axial confining potential leads to deviations from the simple theoretical lineshape given by equation (8).

This sort of interaction with the surface, if controlled, can also be used to cool the trapped atoms. Relaxation of the field gradient reduces the trapping along the dipole beam thus allowing atoms to extend outwards from the trap centre, towards the

prism, coming into contact with the 300 K surface. This interaction with the surface results in loss from the trap, much like the application of an RF knife to selectively remove the most energetic atoms. Carrying out evaporation in this way allows the BEC transition to be reached (see figure 5 (b)) without the need to reduce the dipole intensity further than a first evaporation stage. However, due to the limited and hence inefficient evaporation surface produced by the trapping geometry it was not possible to evaporate to degeneracy solely using this surface technique.

5. Conclusion and outlook

We have demonstrated the successful transport of ultracold ^{87}Rb atoms up to a room-temperature dielectric surface using a combined magnetic and optical trap. We are able to use this transport to fully characterise the variation in trapping potential along the length of the dipole beam quickly and reliably using a single-shot diagnostic technique. Atoms can be positioned at any distance away from the surface by changing the bias field applied which, along with the experimental geometry, provides an excellent starting point for future studies of atom-surface interactions at short-range.

Although the work reported here was performed using ^{87}Rb the experimental apparatus was ultimately designed to produce ^{85}Rb condensates. Here the presence of a broad Feshbach resonance permits the precise tuning of the s-wave scattering length [30], enhancing our control of the condensate. In a first generation of experiments we plan to use bright matter wave solitons, formed by inducing a collapse of the BEC [31, 32], to study classical and quantum reflection [24, 33, 34] from a solid surface in order to gain further insight into the underlying atom-surface potential. The experimental geometry described in this paper facilitates the precise control necessary for such experiments and, in particular, allows low launch velocities of atoms towards the surface. For these types of experiment, solitons have the advantage, not only of being much smaller than the original condensate from which they were formed, but also importantly of being non-dispersive. Both of these factors lead to potentially cleaner reflection signals [35].

The longer term motivation for this apparatus is to use a tunable BEC accurately positioned near to a surface to sensitively measure the atom-surface interaction. A number of interesting measurement schemes have been proposed, including interferometry in a double-well potential [36] and the study of Bloch oscillations in an optical lattice [37], that promise to advance the study of short range forces using ultracold atomic gases.

Acknowledgments

We acknowledge support from the UK Engineering and Physical Sciences Research Council (EPSRC grant EP/F002068/1) and the European Science Foundation within the EUROCORES Programme EuroQUASAR (EPSRC grant EP/G026602/1). SLC acknowledges the support of the Royal Society.

References

- [1] Newton I 1687 *Philosophiæ Naturalis Principia Mathematica* (London: The Royal Society)
- [2] Kramer M, Backer D, Cordes J, Lazio T, Stappers B and Johnston S 2004 *New Astronomy Reviews* **48** 993 – 1002
- [3] Hoyle C D, Schmidt U, Heckel B R, Adelberger E G, Gundlach J H, Kapner D J and Swanson H E 2001 *Phys. Rev. Lett.* **86** 1418–1421
- [4] Masuda M and Sasaki M 2009 *Phys. Rev. Lett.* **102** 171101
- [5] Cavendish H 1798 *Roy. Soc. Phil. Trans.* **88** 469
- [6] Moody M V and Paik H J 1993 *Phys. Rev. Lett.* **70** 1195–1198
- [7] Chiaverini J, Smullin S J, Geraci A A, Weld D M and Kapitulnik A 2003 *Phys. Rev. Lett.* **90** 151101
- [8] Long J C, Chan H W, Churnside A B, Gulbis E A, Varney M C M and Price J C 2003 *Nature* **421** 922
- [9] Kapner D J, Cook T S, Adelberger E G, Gundlach J H, Heckel B R, Hoyle C D and Swanson H E 2007 *Phys. Rev. Lett.* **98** 021101
- [10] Casimir H 1948 *Proc. K. Ned. Akad. Wet* **51**
- [11] Lambrecht A, Neto P A M and Reynaud S 2006 *New Journal of Physics* **8** 243
- [12] Casimir H B G and Polder D 1948 *Phys. Rev.* **73** 360–372
- [13] McLachlan A 1963–1964 *Molecular Physics* **7** 381–388(8)
- [14] Casimir H B G and Polder D 1946 *Nature* **158** 787–788
- [15] Antezza M, Pitaevskii L P and Stringari S 2004 *Phys. Rev. A* **70** 053619
- [16] Dimopoulos S and Geraci A A 2003 *Phys. Rev. D* **68** 124021
- [17] Wolf P, Lemonde P, Lambrecht A, Bize S, Landragin A and Clairon A 2007 *Phys. Rev. A* **75** 063608
- [18] Sandoghdar V, Sukenik C I, Hinds E A and Haroche S 1992 *Phys. Rev. Lett.* **68** 3432–3435
- [19] Onofrio R 2006 *New J. Phys.* **8** 237
- [20] Landragin A, Courtois J Y, Labeyrie G, Vansteenkiste N, Westbrook C I and Aspect A 1996 *Phys. Rev. Lett.* **77** 1464–1467
- [21] Sukenik C I, Boshier M G, Cho D, Sandoghdar V and Hinds E A 1993 *Phys. Rev. Lett.* **70** 560–563
- [22] Bender H, Courteille P W, Marzok C, Zimmermann C and Slama S 2010 *Phys. Rev. Lett.* **104** 083201
- [23] Harber D M, Obrecht J M, McGuirk J M and Cornell E A 2005 *Phys. Rev. A* **72** 033610
- [24] Shimizu F 2001 *Phys. Rev. Lett.* **86** 987–990
- [25] Zhao B S, Schulz S A, Meek S A, Meijer G and Schöllkopf W 2008 *Phys. Rev. A* **78** 010902
- [26] Lin Y J, Perry A R, Compton R L, Spielman I B and Porto J V 2009 *Phys. Rev. A* **79** 063631
- [27] Händel S, Wiles T P, Marchant A L, Hopkins S A, Adams C S and Cornish S L 2011 *Phys. Rev. A* **83** 053633
- [28] Händel S, Marchant A L, Wiles T P, Hopkins S A and Cornish S L *In preparation*
- [29] Harber D M, McGuirk J M, Obrecht J M and Cornell E A *Journal of Low Temperature Physics* **133**(3) 229–238 ISSN 0022-2291
- [30] Cornish S L, Claussen N R, Roberts J L, Cornell E A and Wieman C E 2000 *Phys. Rev. Lett.* **85** 1795–1798
- [31] Donley E, Claussen N, Cornish S, Roberts J, Cornell E and Wieman C 2001 *Nature* **412** 295
- [32] Cornish S L, Thompson S T and Wieman C E 2006 *Phys. Rev. Lett.* **96** 170401
- [33] Druzhinina V and DeKieviet M 2003 *Phys. Rev. Lett.* **91** 193202
- [34] Pasquini T A, Shin Y, Sanner C, Saba M, Schirotzek A, Pritchard D E and Ketterle W 2004 *Phys. Rev. Lett.* **93** 223201
- [35] Cornish S, Parker N, Martin A, Judd T, Scott R, Fromhold T and Adams C 2009 *Physica D: Nonlinear Phenomena* **238** 1299 – 1305
- [36] Chwedeńczuk J, Pezzé L, Piazza F and Smerzi A 2010 *Phys. Rev. A* **82** 032104

- [37] Poli N, Wang F Y, Tarallo M G, Alberti A, Prevedelli M and Tino G M 2011 *Phys. Rev. Lett.* **106** 038501